1 Background

These notes aim to develop a framework for interpreting the X-ray variability typically observed in high-mass binary systems (HMXBs), under the assumption that this variability is due to the propagation of X-rays emitted from the compact object through a clumped stellar wind.

Sect. 2 develops an analytic formalism to predict this intensity-variation, and Sect. 3 a numerical, stochastic clumped wind model for the same objective. Sect. 4 then compares the two approaches.

2 An analytic formulation

2.1 Intensity variance as function of optical depth variance

For a stochastic medium with mean optical depth $< \tau >$ and variance $\delta\tau^2$, let us write the corresponding intensity variance as

$$\delta I^2 =< I^2 > - < I >^2 . \tag{1}$$

Assuming optically thin perturbations we obtain, upon expanding to second order,

$$\delta I^2 \approx I_0^2 e^{-2<\tau>} \delta\tau^2, \tag{2}$$

where I_0 denotes the source intensity, assumed constant throughout these notes. This yields for the normalized rms variation

$$\frac{\delta I}{< I >} \approx \delta\tau, \tag{3}$$

which we note only depends on the perturbation, and not on the mean optical depth.

Figure 1 verifies this optically thin perturbation limit, by plotting the mean intensity and variance from a random-number experiment in which the optical depths for each datum have been drawn from a Gaussian distribution with $< \tau >= 1$. This figure further suggests that a simple modification of the formalism above to

$$< I >\approx I_0 e^{-<\tau>+\delta\tau^2/2}, \tag{4}$$

and

$$\frac{\delta I}{< I >} \approx \delta\tau e^{\delta\tau^2/4}, \tag{5}$$

allows a consideration of also somewhat higher values of $\delta\tau$.

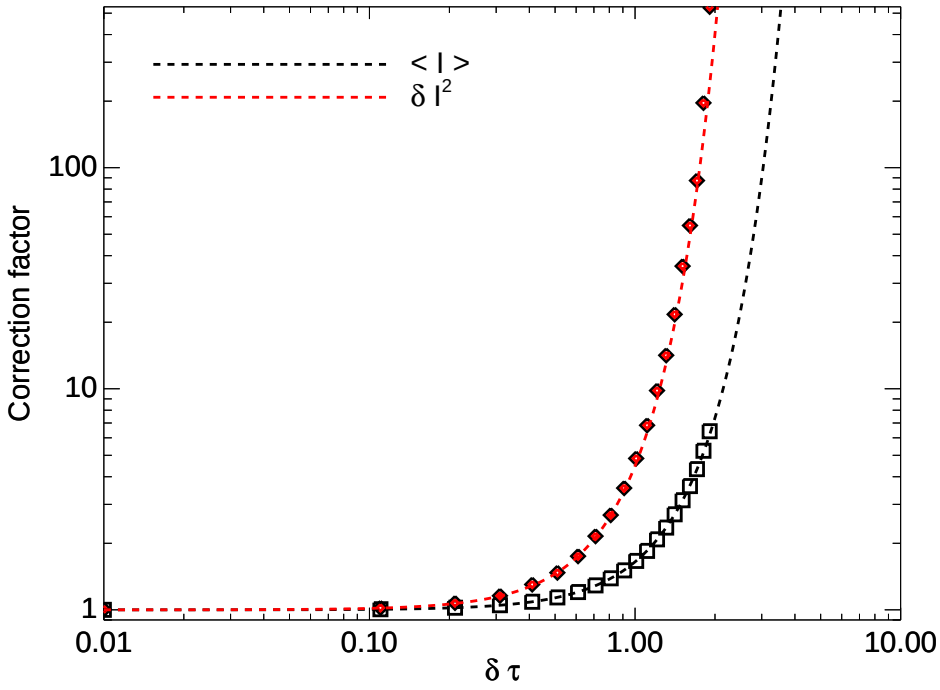

Figure 1: Mean intensities (black squares) and variance (red diamonds) from random-number experiments, see text, as compared to the analytic formulae 4-5. To facilitate the comparisons, both curves have been normalized by multiplying with a factor $e^{<\tau>}$, and the variance further divided by $\delta\tau$.

2.2 Calculating the optical depth variance

Following arguments by Owocki et al. (2009), we write the optical depth variance of X-rays emitted from a source at y_s toward an observer at $y = \infty$ as

$$\delta\tau^2 = \int_{y_s}^{\infty} (\sigma n)^2 h dz, \tag{6}$$

with mean-free-path between clumps h (a.k.a. the 'porosity length'), number density n, and cross-section σ. The equation of continuity then gives for optically thin clumps and 'velocity-stretch' porosity, $h/h_\infty = v/v_\infty$,

$$\delta\tau^2 = \tau_*^2 h'_\infty \int_{z'_e}^{\infty} 1/(v' r'^4) dz', \tag{7}$$

where primed quantities have been scaled to the stellar radius and terminal speed, respectively. Note here that this model predicts the X-ray luminosity variation should depend only on the porosity length h and on the stellar and wind parameters, via $\tau_* \equiv \dot{M}\kappa/4\pi R_\star v_\infty$, but *not* on the clump length scales.

NOTE: I do wonder about clumping, though, considering the integral we're solving.

In principle, we can now numerically integrate eqn. 7 to obtain general predictions for $\delta\tau$ as a function of orbital phase of the emitting source, for quite arbitrary velocity-fields and orbital motions.

However, in spherical symmetry and for 'β-type' velocity-laws $v = v_\infty(1 - 1/r')^\beta$ with integer values of β, eqn. 7 can also be solved analytically. So let us thus first consider the constructive example of an X-ray source located at inferior conjunction, and embedded in a clumped wind with a $\beta = 1$ velocity law. Then

$$\delta\tau^2 = \tau_*^2 h'_\infty \int_{r'_s}^{\infty} \frac{1}{r'^4 - r'3} dr' = \tau_*^2 h'_\infty \left(-\frac{2r'_s + 1}{2r'^2_s} + \ln \frac{r'_s}{r'_s - 1} \right). \tag{8}$$

For typical values $r'_s = 3$, $\tau_* = 0.1$, and $h'_\infty = 1$, eqn. 8 yields $\delta\tau^2 \approx 1.7 \times 10^{-4}$, which we will see later actually is in quite good agreement with the variance in numerical, stochastic wind models, which we now discuss.

3 Numerical simulations of a stochastic, clumped wind

3.1 General set-up

This section describes a method for calculating HMXB X-ray light-curves as functions of orbital phase, by shooting rays from a point-source within a stochastic, clumped stellar wind. The stochastic wind is constructed by following the radial expansion of mass-conserving clumps (essentially as in Sundqvist et al. 2012, their Appendix A), and again assuming a velocity-stretch form of the

porosity, $h/h_\infty = v/v_\infty$. Using then the definition of the porosity length as the mean-free-path between clumps,

$$h(r) \equiv \frac{1}{n_{\rm cl} A_{\rm cl}} \tag{9}$$

such mass-conserving clumps demand

$$n_{\rm cl} \sim \frac{1}{r^2 v} \sim \frac{1}{A_{\rm cl} h} \sim \frac{1}{A_{\rm cl} v}, \tag{10}$$

and so $A_{\rm cl} \sim r^2$. Assuming isotropic opacity, we thus create a wind consisting of spherical clumps of radius $r_{\rm cl}$ that expand from some surface value $r^*_{\rm cl}$,

$$r_{\rm cl}(r) = r^*_{\rm cl} r', \tag{11}$$

where r' again denotes the scaled stellar radius.

Note that the volume filling factor is not constant within this model, but varies as $f_{\rm vol} \sim r/v$. Thus, in the outer wind clumps will start to overlap and $f_{\rm vol}$ may reach values above unity; physically, this stems from the assumed velocity-stretch porosity, which requires constant mfp's between 'clump-centers' when the terminal speed is reached, whereas the mass-conserving clumps continue to expand.

The accumulative number of clumps contained in a volume from onset radius $R_{\rm min}$ to maximum radius $R_{\rm max}$ is,

$$N_{\rm tot} = 4\pi \int_{R_{\rm min}}^{R_{\rm max}} n_{\rm cl} r^2 dr = \frac{4R_*^3}{h_\infty (r^*_{\rm cl})^2} \int_{R_{\rm min}}^{R_{\rm max}} \frac{1}{v'} dr'. \tag{12}$$

For integer β velocity laws, this can again be analytically integrated, and yields for a $\beta = 1$ field with typical values $r^*_{\rm cl} = 0.01 R_*$ (about a Sobolev length), $h'_\infty = 1$, $R_{\rm min} = 1.2$, and $R_{\rm max} = 300$, $N_{\rm tot} = 12.2$ million (!) clumps. (Of course, many of these clumps are located at very large radii, and so contribute negligibly to the X-ray optical depth.)

3.2 Clump generation method

A random set of $N_{\rm tot}$ clumps with the required statistical distribution in radius is drawn by generating a set of pseudo-random numbers distributed as $\sim 1/v'$. For a $\beta = 1$ law, the normalized cumulative distribution function can then be inverted in terms of the ProdoctLog function (see Sundqvist et al. 2012). But to be somewhat more general, we here instead use the numerical Von-Neumann acceptance-rejection method (e.g. Press et al. 1992) to generate the required distribution in r'. Using the assumed statistical spherical symmetry, the corresponding random clump co-latitudinal cosine μ and azimuth ϕ are trivially found.

With the clump-positions in hand, we next shoot X-rays from a source located at some position $X_{\rm orb}, Y_{\rm orb}, Z_{\rm orb}$ within the wind, and search for clumps

between this source and an observer at $Y = -\infty$. For simplicity, these notes consider only orbits in the $Z = 0$ plane, and so we can speed up this clump-search by considering only the plane $|\mu| \leq 2r^*_{\rm cl}$.

Whenever the ray pierces a clump, the 'clump impact parameter' $p^2_{\rm cl} = (Z_{\rm orb} - Z_{\rm cl})^2 + (X_{\rm orb} - X_{\rm cl})^2$ determines the path length $l_{\rm cl} = 2\sqrt{r^2_{\rm cl} - p^2_{\rm cl}}$ through this clump. Since the average path-length is $< l >= 4r_{\rm cl}/3$, we for clumps of constant internal density also get the mean optical depth

$$< \tau_{\rm cl} >= \kappa\rho_{\rm cl} < l >= \kappa < \rho > h = \tau_* h'_\infty / r'^2, \tag{13}$$

and so the optical depth of any such 'limb-brightened' clump with impact parameter $p_{\rm cl}$ at radius r' may be conveniently expressed as

$$\tau_{\rm cl} =< \tau_{\rm cl} > \frac{3}{2}\sqrt{1 - \frac{p^2_{\rm cl}}{r^2_{\rm cl}}}. \tag{14}$$

The total optical depth is then obtained by simply summing up the contributions from all individual clump-hits. Figure 2 compares the optical depth-curve of a smooth wind with those calculated using the stochastic model described above, showing good agreement when the latter is averaged over many wind-renditions.

4 Comparison of the analytic and numerical models for X-ray variability

Let us now compare the analytic and numerical models developed in Sects. 2 and 3.

Figure 3 illustrates numerical intensity-curves for different porosity-lengths and clump-radii, and confirms the basic expectation that the variance should be more dependent on the former quantity.

Figure 4 then compares standard deviations in normalized intensity calculated from the analytic and numerical models. It shows the two approaches agree well, except for close to occultation, where the assumed clump-onset radius at $R_{\rm min} = 1.2$ in the numerical model most likely plays a role for the variability-drop (such an on-set radius has not yet been included in the analytic model-calculations). The figure moreover confirms the analytic expectation that the variability is relatively insensitive to the clump-sizes, however a small dependence is still visible in the numerical simulations.

In summary, these developments seem to suggest that a good way to study HMXB-variability may be during phases close to inferior conjunction (or systems with higly inclined orbits), in order to reduce as much as possible effects from near-star regions (as well as optical depth effects).

4.1 Optically thick

Not yet...

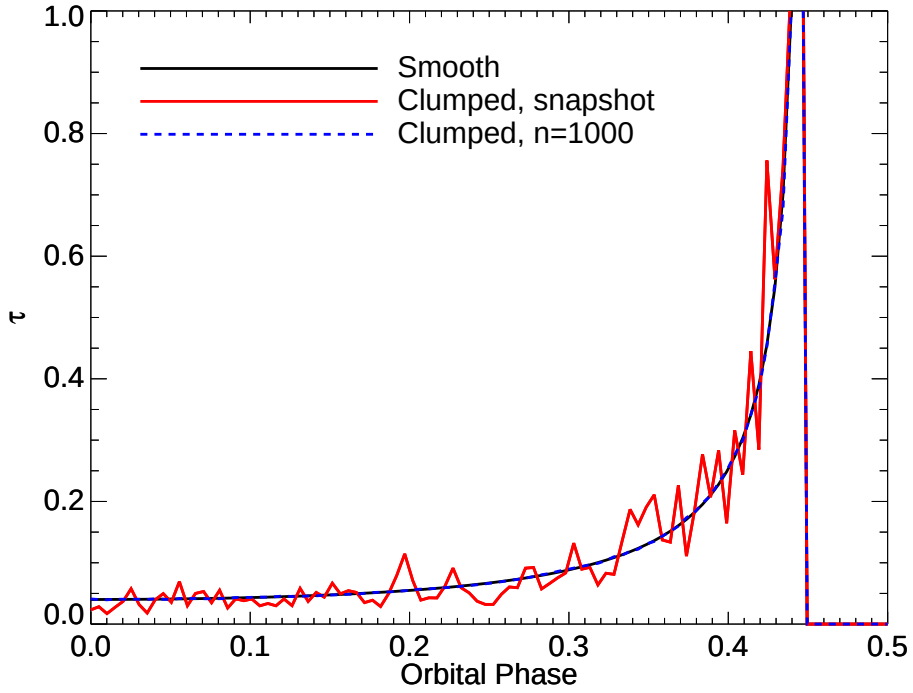

Figure 2: Comparison of optical depth curves for X-rays emitted by a point-source in circular orbit at $r = 3R_*$, when these propagate through an optically thin ($\tau_* = 0.1$) smooth (black) vs. clumped (red, $h'_\infty = 1$) wind. The clump-averages have been calculated from 1000 renditions of the wind, the source is at inferior conjunction at phase 0, and the optical depth has for simplicity been set to zero when the source goes into occultation behind the star.

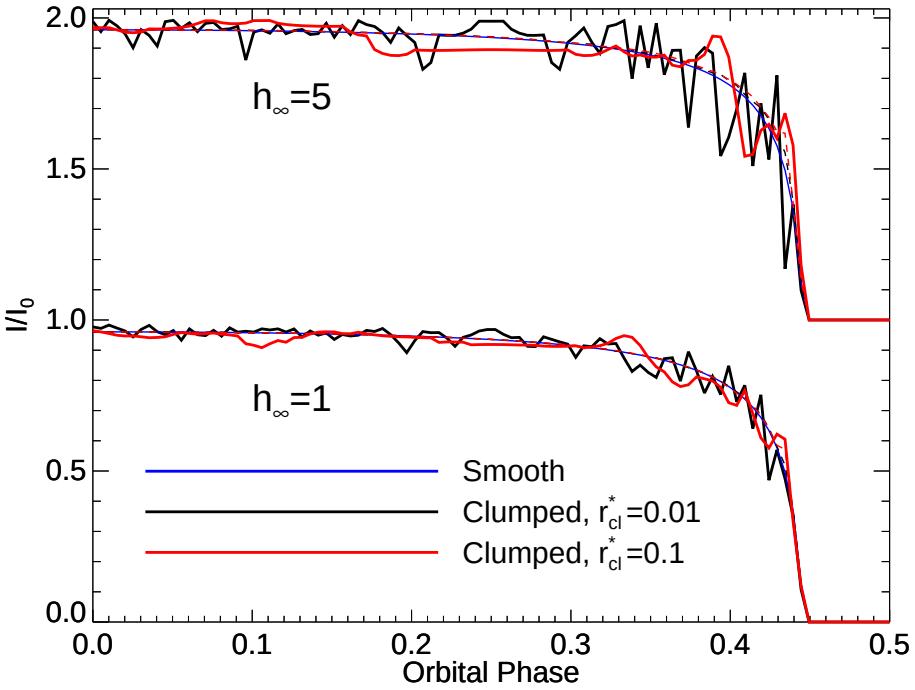

Figure 3: Intensity as function of orbital phase, for the same orbit and $\tau_* = 0.1$ simulation as in figure 2, but now for two different porosity-lengths (upper and lower panels, upper shifted by +1), and two different clump-radii (black and red curves), as given in figure. Solid curves computed from one snapshot wind-rendition, and dashed curves averaged over 1000 such renditions.

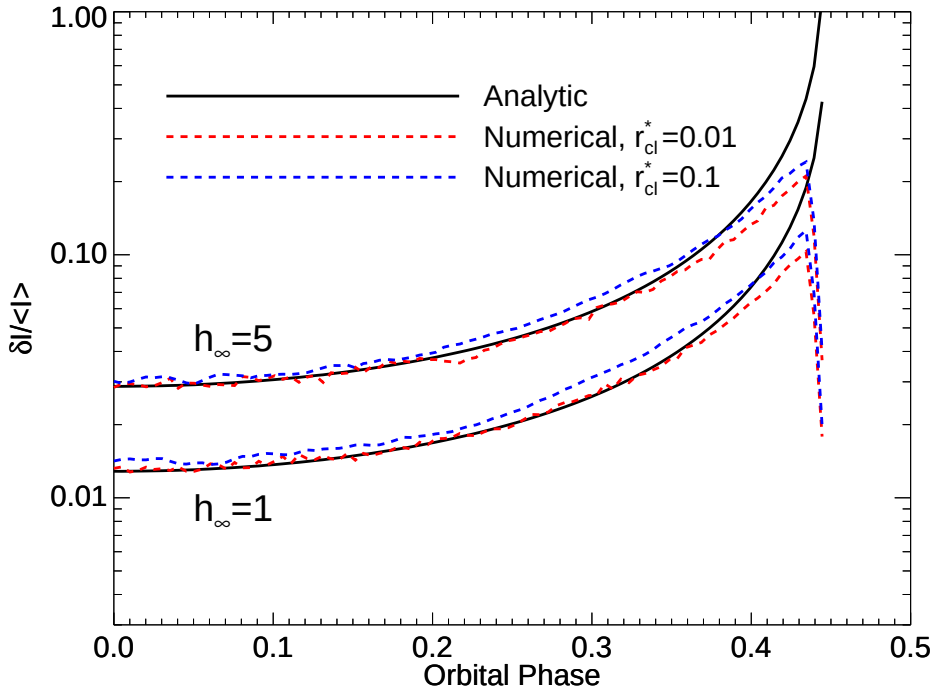

Figure 4: Intensity standard deviations predicted by the numerical and analytic models developed in these notes, for the same parameters as in figure 3.

4.2 Time-scale of intensity variability

Not yet...

But note that figure 3 seems to support the qualitative expectation that the intensity variance time-scale should be longer for larger clumps. Quite generally, we may expect the correlation between the intensity variance at two positions in the orbit be zero for length-scales larger than $2d_{\rm cl}$.

Thus, may these time-scales give some clues regarding typical clump-length scales?

5 X-ray colour

Not yet...

6 Variability using dynamical 2-D LDI simulations

Not yet...